Talanta 204 (2019) 20–28

Contents lists available at ScienceDirect

Talanta

journal homepage: www.elsevier.com/locate/talanta

An rGONS-based biosensor for simultaneous imaging of p53 and p21 mRNA in living cells

Jialong Fan[a,1], Chunyi Tong[a,1], Wenya Dang[a], Yan Qin[b], Xuanming Liu[a], Bin Liu[a,*], Wei Wang[b,**]

[a] College of Biology, Hunan Province Key Laboratory of Plant Functional Genomics and Developmental Regulation, Hunan University, Changsha, 410082, China
[b] TCM and Ethnomedicine Innovation & Development International Laboratory, Innovative Material Medical Research Institute, School of Pharmacy, Hunan University of Chinese Medicine, Changsha, 410208, China

ARTICLE INFO

Keywords:
rGONS
mRNA
p53
p21
Cell imaging
Nanosystem

ABSTRACT

Hepatocarcinoma is the second leading cause of cancer-related death worldwide accompanied by the aberrant expression of many genes. Among of them, p53 and p21 genes played a vital role in the development of liver cancer. Thus, monitoring mRNA levels of the two markers is urgently needed for early diagnosis and understanding the molecular mechanism of hepatocarcinoma development. Herein, a functional nanosystem for in situ and real-time monitoring levels of p53 and p21 mRNA was constructed using reduced graphene oxide nanosheet assisted fluorescence probes. Comparing with traditional methods, the new method indicated high sensitivity and outstanding selectivity towards p53 and p21 mRNA assay *in vitro*. Moreover, the functional nanosystem was successfully used for monitoring dynamic change of mRNAs in HepG2 cells caused by cisplatin treatment, the reliability of which was confirmed by RT-PCR. In summary, this strategy provides a promising tool to reveal p53 and p21 mRNA regulatory process in cancer cells, which is practicable for drug screening and therapy evaluation on clinic.

1. Introduction

Hepatocarcinoma, the second leading cause of death from cancer (9%), is seriously threatening to human health [1,2]. Until now, no obvious symptom was found in the early stage of this kind of tumor. However, abnormal expression and mutation of multiple genes often appeared in this kind of tumor at early stage [3,4]. Thus, developing an efficient and simple method for mRNA assay is helpful for improving the early diagnosis. As a tumor suppressor, p53 plays an important role in regulating cell cycle arrest, apoptosis, DNA repair, autophagy et al. [5]. The aberrant expression of p53 mRNA played a vital role in the development of hepatocarcinoma [6,7]. In addition, p21, a transcriptional target of p53, is also associated with the development and prognosis of hepatocarcinoma by mediating cell cycle and apoptosis. Hence, real-time monitoring mRNA level of the two genes can provide reliable evidence for the early diagnosis. Although many developed techniques, including Northern blot [8], DNA microarrays [9], in situ hybridization [10] and RT-PCR [11,12], has been used for *in vitro* mRNA assay, monitoring of cellular mRNA *in vivo*, which can dynamically reveal the spatial and temporal variations of mRNA, is still scarce due to the weak and/or unspecific signal output in some extent. Therefore, a more reliable analysis platform for real-time monitoring mRNA in living cells would be of particular significance.

Recently, Sensors based on different nanomaterials, have been widely used for biomolecular detection [13,14], heavy-metal ion detection [15,16], water quality monitoring [17,18] et al. Among of these nanomaterials, graphene oxide (GO), a 2D carbon nanomaterial, has attracted wide attention due to its remarkable electronic, mechanical and thermal properties [19–21]. Many evidences have indicated that GO can efficiently quench the fluorescence signal of single-stranded DNA (ssDNA) through π-π stacking, while the signal can be restored by formation of double-stranded DNA (dsDNA) due to the weak interaction between GO and dsDNA [22]. Although it has been reliably and sensitively used for nucleic acid assay *in vitro,* the inherited toxicity of GO to cells and tissues directly defined its limited application *in vivo* [21,23]. However, the reduced graphene oxide (rGO) showed a significant advantage of ultra-low toxicity [24,25]. Meanwhile, this kind of nanomaterial with less hydrophilic edge groups is principally internalized by phagocytic uptake in cells, making intracellular imaging of target genes possible [26]. In addition, the stronger adsorption and

* Corresponding author.
** Corresponding author.
E-mail addresses: binliu2001@hotmail.com (B. Liu), wangwei402@hotmail.com (W. Wang).
[1] These authors contributed to the work equally and should be regarded as co-first authors.

https://doi.org/10.1016/j.talanta.2019.05.087
Received 17 February 2019; Received in revised form 15 May 2019; Accepted 20 May 2019
Available online 24 May 2019
0039-9140/

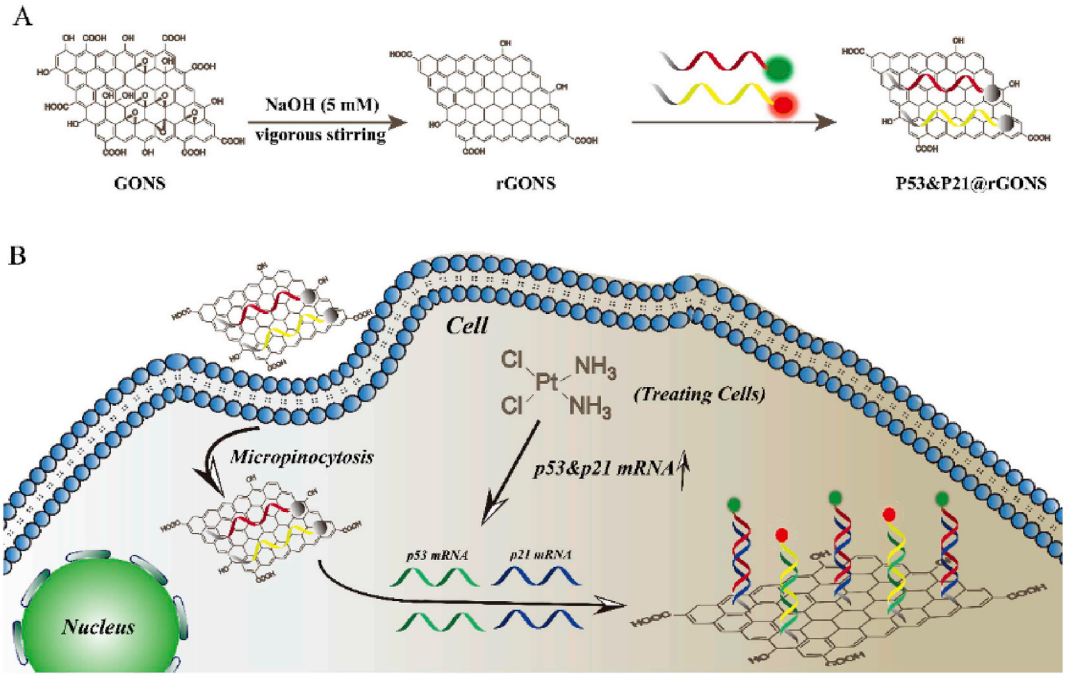

Scheme 1. (A) Preparation of functional DNA strands-immobilized rGONS (P53&P21@rGONS) nanosystem. (B) Illustration of the P53&P21@rGONS nanosystem for mRNA imaging *in vivo* via the target-triggered specific hybridization.

fluorescence quenching capability are also helpful for mRNA image *in vivo* relative to GO [27].

In this work, we applied rGO for simultaneously monitoring p53 and p21 mRNA in living cells by adsorbing FAM-labeled p21 probe (P21) and Cy5-labeled p53 probe (P53) on the surface. After the two fluorescence probes hybridize with corresponding targets through base pairing, the formation of DNA/RNA duplexes directly result in the release of probes from the surface of rGONS and accordingly restore fluorescence signal (Scheme 1). Based on this principle, we established a fluorescence 'off/on' method for simultaneous imaging of dual genes *in vivo*.

2. Experimental section

2.1. Chemicals and apparatus

DNA oligonucleotides were synthesized and purified by HPLC (Takara Biotechnology Inc., Dalian) and the sequences are listed in Table 1. The GO powder was purchased from Xianfeng Nanotechnology Co., Ltd (Nanjing, China). Deoxyribonuclease I (DNase I) was purchased from Solarbio Science and Technology (Beijing, China). All solutions including hybridize buffer solution (50 mM Tris-HCl, 15 mM $MgCl_2$, 1 mM EDTA, pH 7.5) were prepared using MilliQ water by a Milli-Q Plus System (Millipore Corp., USA). Dulbecco's Modified Eagle Medium (DMEM), fetal bovine serum (FBS), penicillin, streptomycin and other chemicals were purchased from Sigma (Milan, Italy). Mouse anti-rabbit IgG-p21 and p53 (sc-397, sc-6243) were purchased from Santa Cruz. All cell lines were purchased from Xiangya Central Laboratory, Central-South University.

Table 1
Sequences of oligonucleotides.

Name	Sequence (5′-3′)	Number of bases
P53	TTTTTTTTTGCACAAACACGCACCTCAAAGC-Cy5	31
P21	TTTTTTTTTAGGACACATGGGGAGCCGA-FAM	28
scDNA	TTCTTTCTTCCCTTGTTTGTT-FAM	21
T_{53}	GCUUUGAGGUGCGUGUUUGUGC	22
T_{21}	UCGGCUCCCCAUGUGUCCU	19
T_{VEGF}	CAUCACCAUGCAGAUUAUGCG	21
T_{HCV}	GCUCCACUGGCAAGGCCUGG	20
T_{miR-21}	CAACAUCAGUCUGAUAAGCU	20
F-p21-primer	ACCTTCCAGCTCCTGTAACATACT	24
R-p21-primer	GTCTAGGTGGAGAAACGGGAA	21
F-p53-primer	ATGAGCCGCCTGAGGTTGG	19
R-p53-primer	CAGCCTGGGCATCCTTGAGT	20
F-β-action-primer	TCCGTGGAGAAGAGCTACGA	20
R-β-action-primer	GTACTTGCGCTCAGGAGGAG	20

The fluorescence measurement was performed on the FL-7000 Fluorescence spectrophotometer (Hitachi, Japan). Fluorescence imaging was obtained using FV1000-IX81 Laser scanning confocal microscopy (OLYMPUS, Japan). Zeta potential was recorded using a Zeta sizer (Malvern Nano series, Malvern, UK). The FT-IR spectra were determined on a Nicolet 6700 FT-IR spectrophotometer (Thermo Fisher Scientific Inc, USA). UV–Vis absorption was determined on the DU800 spectrophotometer (Beckman Coulter Inc, USA). MTT assay was measured using microplate reader (PerkinElmer, USA). Fluorescent images were collected using small animal multi-mode imaging system (luminaxr, US).

2.2. Optimization of reaction conditions between probe and rGONS

GO powder was prepared as described previously [22]. Solutions of 100 nM FAM-labeled p21 probe (P21) and Cy5-labeled p53 probe (P53) were incubated with various concentrations of rGONS for 10 min at room temperature before the fluorescence intensities of samples were measured. Kinetic study of fluorescence quenching was carried out as follows: after adding different concentrations of rGONS to the solution of 100 nM P53 and P21, respectively, the fluorescence signal was recorded on the fluorescence spectrophotometer for 20 min. The excitation wavelength of P53 and P21 were 635 nm and 450 nm, respectively. The emission wavelengths of P53 and P21 were in the range from 655 to 700 nm and 500–600 nm, respectively.

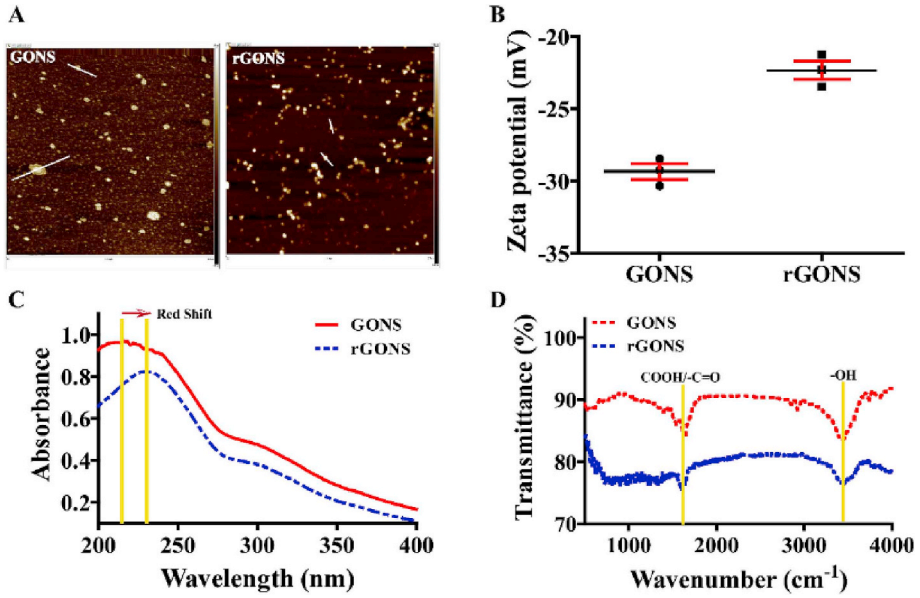

Fig. 1. Comparison of physicochemical properties of GONS and rGONS. (A) AFM image of GONS and rGONS. (B) Zeta potential of GONS and rGONS. (D) UV–vis spectrum of GONS and rGONS. (E) FT-IR spectrum of GONS and rGONS.

2.3. mRNA detection using P53&P21@rGONS platform

The probe@rGONS nanosystem was prepared by mixing 50 nM P53 and 50 nM P21 with 6 μg/mL of rGONS in the reaction solution. T_{53} and T_{21} with different concentrations were added into the nanosystem and incubated for 30 min at 37 °C. Then, the fluorescence intensities were measured. In dual targets detection, 100 nM P53 and 100 nM P21 were mixed with 12 μg/mL rGONS, followed by addition of 100 nM T_{53} or 100 nM T_{21} mRNA. In addition, the specificity of the method was investigated by incubating the nanosystem with 100 nM T_{21}, T_{53}, T_{VEGF}, T_{HCV} and $T_{miR\text{-}21}$ at 37 °C for 30 min, separately, before measuring fluorescence intensity.

2.4. Cytotoxicity assay of rGONS

Liver cancer cell lines of HepG2, SMMC-7721 and BEL-7404 were seeded in the 96-well microplate (5×10^4 cells/well) and cultivated for 24 h. Then, rGONS (0–50 μg/mL) was added and incubated for 12 h at 37 °C. Following with rGONS treatment, cells were washed 3 times with PBS and incubated with 100 μL MTT (0.5 mg/mL) at 4 h. After discarding the medium, 150 μL of DMSO was added to record the absorbance at 490 nm on the microplate reader.

2.5. Uptake assay of rGONS

After rGONS (1 mg/mL) has interacted with Rhodamine 6G (RDM) (Fluka) for 12 h, 10 KD filter was used to remove excess RDM from rGONS. HepG2 cells seeded on the 12-well plates (5×10^5 cells/well) were cultivated for 24 h, followed by PBS washing. Three kinds of small-molecule inhibitors were respectively added and incubated for 1 h. Finally, rGONS-RDM (10 μg/mL) was added and incubated for another 4 h. Meanwhile, Hoechst 33342 was added to stain cell nuclear.

2.6. mRNA detection in live cells

HepG2 cells were seeded on the 12-well plate with a density of 5×10^5 cells/well. Cisplatin was used to induce p21 and p53 mRNA expression in HepG2 cells. In a single target detection group, P21@rGONS complex was incubated with liver cancer cells under 1% FBS for 10 h at 37 °C. In the dual targets assay, P21&P53@rGONS nanosystem with different concentrations was added to HepG2 cells after treatment with cisplatin. Fluorescence intensity of FAM and Cy5 were obtained under laser scanning confocal microscope.

2.7. qRT-PCR assay

Cellular total RNA was isolated using TRIzol reagent. cDNA synthesized using an iScript kit (Bio-Rad) was used as the template in the following PCR reaction. The PCR reaction procedure was carried out as follows: 5 min at 95 °C, (30 s at 95 °C, 30 s at 55 °C and 30 s at 72 °C) × 40 cycles, 10 min at 72 °C using Bio-Rad real-time PCR system.

2.8. Western blotting

Cells were lysed in the RIPA buffer containing Phenylmethanesulfonylfluoride. Samples were separated using SDS-polyacrylamide gel electrophoresis and transferred into polyvinylidene fluoride membrane. The membranes were blocked with 5% skim milk in Tris-buffered saline with Tween-20 and incubated with antibodies against p21, p53 or β-actin overnight at 4 °C, followed by incubating with HRP-conjugated secondary antibodies. The blots were visualized using BIO-RAD ChemiDoc XRS chemiluminescence system.

3. Results and discussion

3.1. Characterization of rGONS and feasibility of the mRNA detection system

rGONS nanosheets were synthesized through the reduction of GONS. AFM images indicated that the thickness and the size of control GONS were of ~1.5 nm and 80–150 nm, respectively, which is consistent with previous reports Although the thickness of rGONS remains stable, the size decreased to 50–80 nm after with reduction treatment (Fig. 1A and Fig.S1. Zeta potential assay indicated a higher potential of rGONS (−22 mV) comparing with GONS (−28 mV) (Fig. 1B), due to the decrease of oxygen groups on the surface. Meanwhile, reduction treatment of GONS resulted in the shift of maximal absorption from 218 nm to 231 nm (Fig. 1C), which is consistent with previous report [25]. In addition, FT-IR showed that the sharp peak of C═O/COOH at 1652 cm^{-1} and the broad peak of –OH around 3400 cm^{-1} for GONS was stronger relative to rGONS (Fig. 1D). These data clearly confirmed the successful synthesis of rGONS.

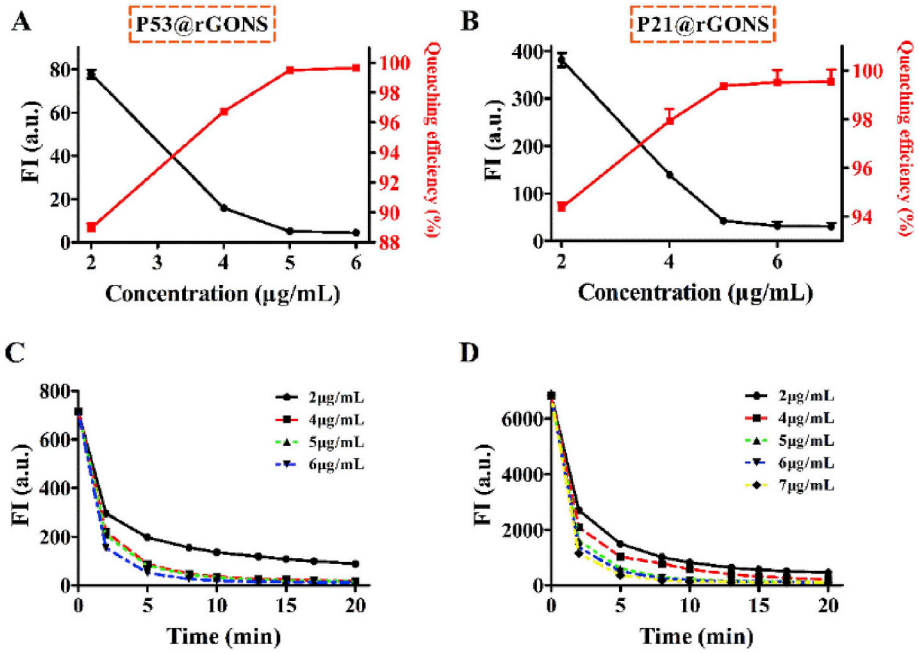

Fig. 2. Comparison of the relationship between fluorescence signal and quenching efficiency of P53 and P21 under different concentration of rGONS. (A, B) Fluorescence single changes of P53 and P21 with different concentration of rGONS. (C, D) The fluorescence intensities of P53@rGONS (C) and P21@rGONS (D) nanosystem at different time point.

3.2. The condition optimization of rGONS

As the quenching ability of rGONS to fluorescence probe is related to concentration and reactive time [28], We then investigated the effect of rGONS concentration on the quenching efficiency of fluorescence probes and found that the fluorescent signal of probes decreased in an rGONS concentration-dependent manner and both of the quenching efficiency was more than 99% at the presence of 6 μg/mL rGONS (Fig.S2, Fig. 2A and B). In addition, it has been reported that the lower energy level of rGONS can increase the efficiency of electron transfer from the dyes to rGONS comparing with GONS [29], which was reflected by the increase of quenching speed and the shortening of time for reaching the plateau of fluorescence quenching rate (Fig. 2C and D). In addition, other condition optimization of Mg^{2+} concentration, reaction time and temperature referred to the data of our previous study [22,30].

3.3. The S/B assay

In order to investigate the feasibility of the strategy, we monitored the signal change of probes caused by the different target. As shown in Fig. 3, the tight adsorption of P53 or P21 probe on the rGONS surface resulted in strong fluorescence quenching while the presence of corresponding targets caused the increase of fluorescence signal about 40-fold (Fig. 3A and B) and 50-fold (Fig. 3C and D) due to the weak interaction between hybrids and rGONS. Comparing with common, molecular beacon(S/B ratio < 20) [31], the above results demonstrated the higher S/B ratio of rGONS-based fluorescence probe, which can be attributed to the ultra-low background of the system.

3.4. In vitro detection of p21/p53 mRNA

We next studied the effect of mRNAs concentration on the fluorescence change of the nanosystem. Fig. 4A and B indicated that the fluorescence signal increased as the target mRNAs concentrations varied from 0 to 100 nM. Moreover, the concentration of two targets and the corresponding fluorescence intensity indicated a good linear relationship in the range from 0 to 100 nM (Fig. 4C and D). Based on the standard curve, two regression equations for y = 2.6294x - 4.1757 (T_{53}, C) and y = 6.4082x - 19.74 (T_{21}, D) were obtained, where y represents the fluorescence intensity of 665 nm (T_{53}) and 522 nm (T_{21}), x indicates the target concentration. The detection limits for p53 mRNA and p21 mRNA were calculated to be 0.71 ± 0.053 nM and 0.46 ± 0.045 nM (detection limit (DL) = 3.3 × (standard deviation/slope of the calibration curve)) [32], respectively. Comparing with previous report [33,34], the new detection system based on rGONS exhibited acceptable performance for mRNA detection. In addition, we further studied the regeneration of the nanosystem for the potentiality. As shown in Fig.S3, the results indicated that hybrid duplex can be digested with 0.1 μg/mL RNase A while releasing probe, which was resorbed by rGONS (decrease in fluorescence intensity). Therefore, the detection system we designed has the possibility of regenerative ability.

3.5. Selectivity investigation of the rGONS-quenched probe for mRNA detection

The selectivity ability was further assessed by comparing the fluorescence signal of the nanosystem at the presence of different targets. As shown in Fig. 5A and B, both of T_{21} and T_{53} caused the increase of significant fluorescence signal at 521 nm, while no obvious signal increase was found when other DNA/RNA targets containing unrelated sequences were present, due to the lack of hybridization between probe and target. In addition, in situ imaging result obtained from IVIS imaging system in Fig. 5C indicated the significant increase when the two probes hybridized with the corresponding mRNA. Meanwhile, no cross interference was observed for the two probes. Therefore, the new nanosystem is feasible for detecting target mRNA under complex environment.

3.6. Stability and cell viability assay of nanosystem/rGONS

Several kinds of nanomaterial inherited the strong anti-nuclease ability, which can efficiently avoid the disturbance of nucleases when the DNA probe was used for cell imaging [34,35]. In this study, we also found that negligible change of the fluorescence signal of the two nanosystems was observed after with DNase I or cell-free extracts treatment (Fig. 6A and B). Only the addition of corresponding targets can recovery the fluorescence signal (Fig. 6C and D). In addition, PAGE assay directly confirmed the anti-nuclease ability of P53@rGONS and P21@rGONS nanosystem (Fig.S4). The characteristic of anti-nuclease

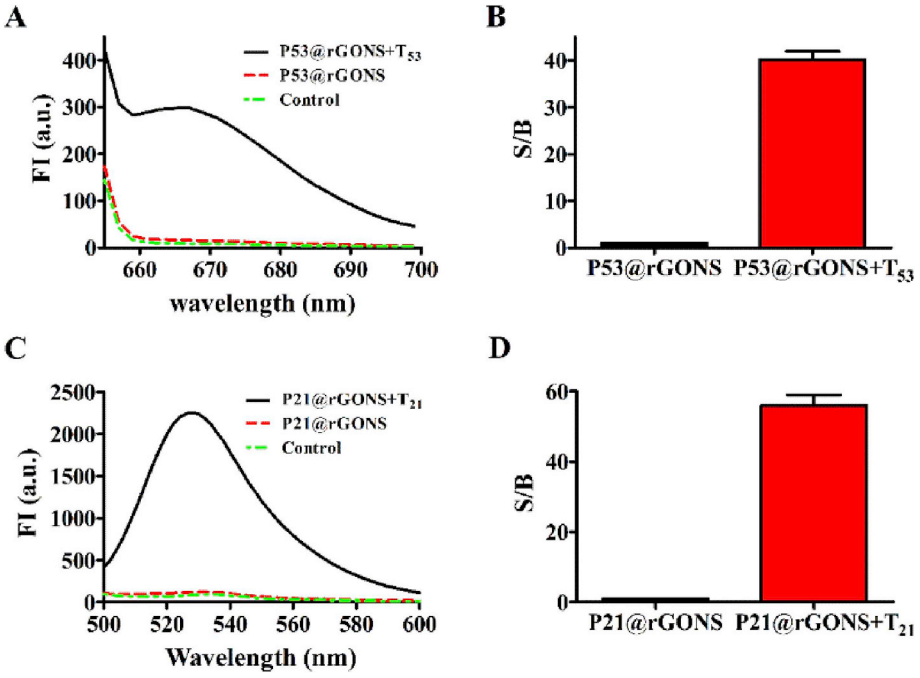

Fig. 3. Feasibility analysis of the detection system. (A, C) The fluorescence emission spectra of P53@rGONS and P21@rGONS in the absence/presence of T_{53} and T_{21}, respectively. (B, D) Comparison of the signal-to-background ratio (S/B) of two probe@rGONS in the absence and presence of excess T_{53} and T_{21}, respectively.

digestion demonstrated the practical applicability of this nanosystem for mRNA imaging in living cells without the distribution of unspecific nuclease degradation.

In addition, MTT assay was used to evaluate the cytotoxicity of rGONS to the tumor cells. As shown in Fig.S5, all investigated cancer cells showed more than 90% viability after incubating with high concentration of rGONS (50 μg/mL) for 12 h. Moreover, the viability of investigated cell lines was more than 95% with the presence of 10 μg/mL rGONS. By combining with our previous results that rGONS with concentration less than 12.5 μg/mL did not affect gene mRNA expression [36], it can be concluded that the rGONS is suitable for *in vivo* application without disturbing gene expression.

3.7. Uptake mechanism of rGONS

In addition, we also explored the cell uptake mechanism and the located region of rGONS by using RDM as the indicator. Fig. 7A indicated that all investigated inhibitors showed an inhibitory effect on cell uptake of rGONS-RDM. Among of them, uptake efficiency of rGONS reduced about 95% ± 2.4% in the presence of rottlerin while little difference was observed between β-cyclodextrins and chlorpromazine treatment group (Fig. 7B). As rottlerin, β-cyclodextrins and

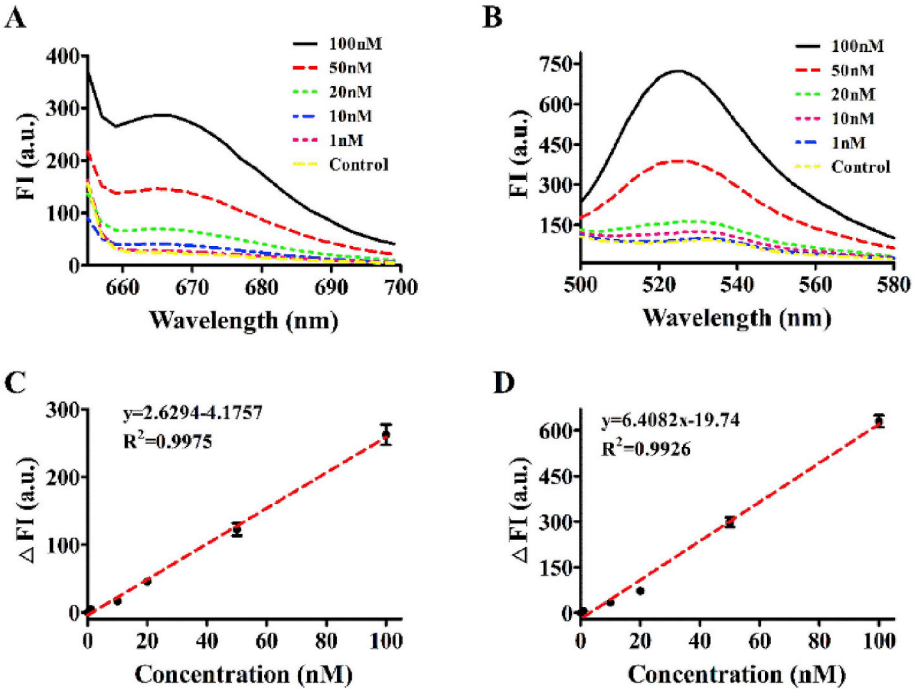

Fig. 4. (A, B) Fluorescence emission spectra of the P53&P21@rGONS sensing platform in the presence of T_{53} (A) and T_{21} (B) with different concentrations. (C, D) The standard curve of absolute fluorescence intensity (△FI) *VS* concentration detection of T_{53} (C) and T_{21} (D) from 0 nM to 100 nM.

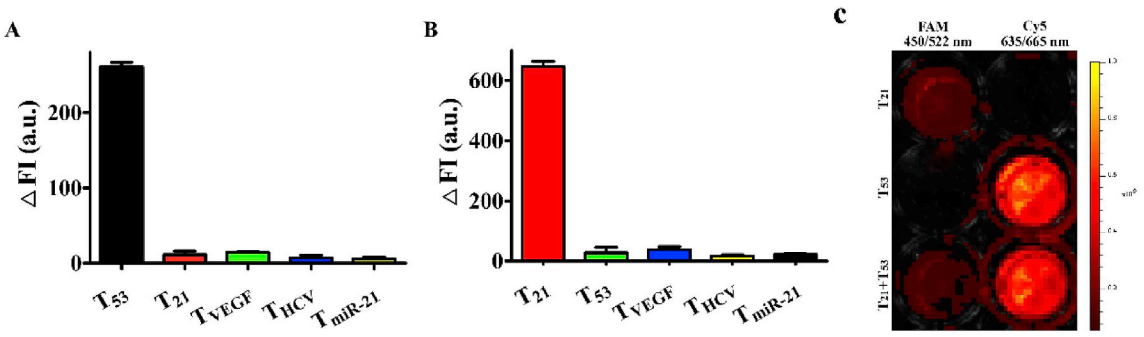

Fig. 5. (A, B) Fluorescence intensity responses of the nanosystem measured at excitation wavelengths of 665 nm (A) and 522 nm (B). (C) Simultaneous detection of dual mRNA *in vitro*.

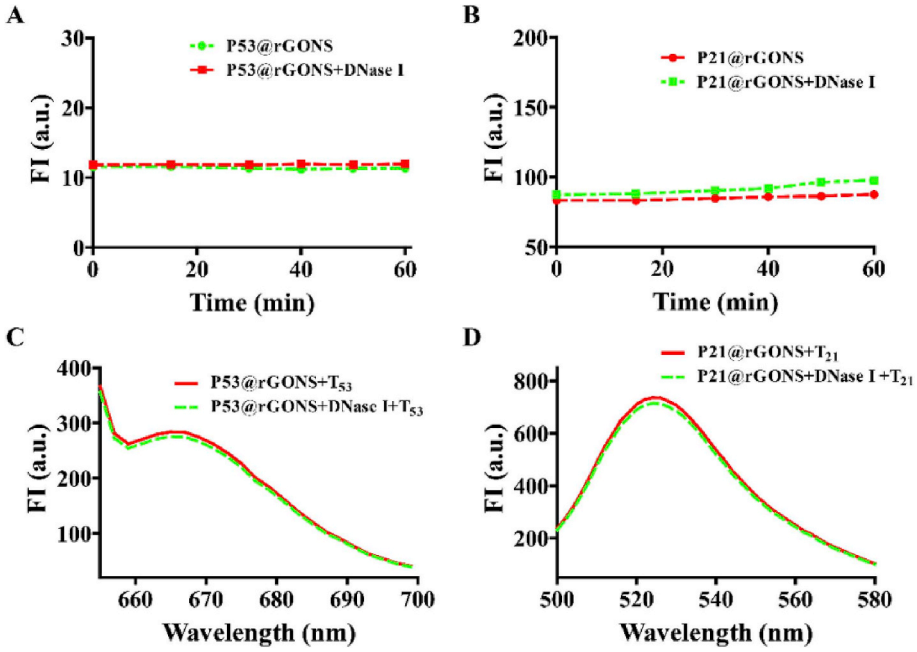

Fig. 6. Nuclease stability of the nanosystem. (A) Fluorescence signal curve of P53@rGONS in the buffer without or with DNase I as a function of time. (B) Fluorescence signal curve of P21@rGONS in the buffer with DNase I or not as a function of time. Fluorescence spectra after hybridization of the P53@rGONS (C) and P21@rGONS (D) with target mRNA in the absence of DNase I and the presence of DNase I.

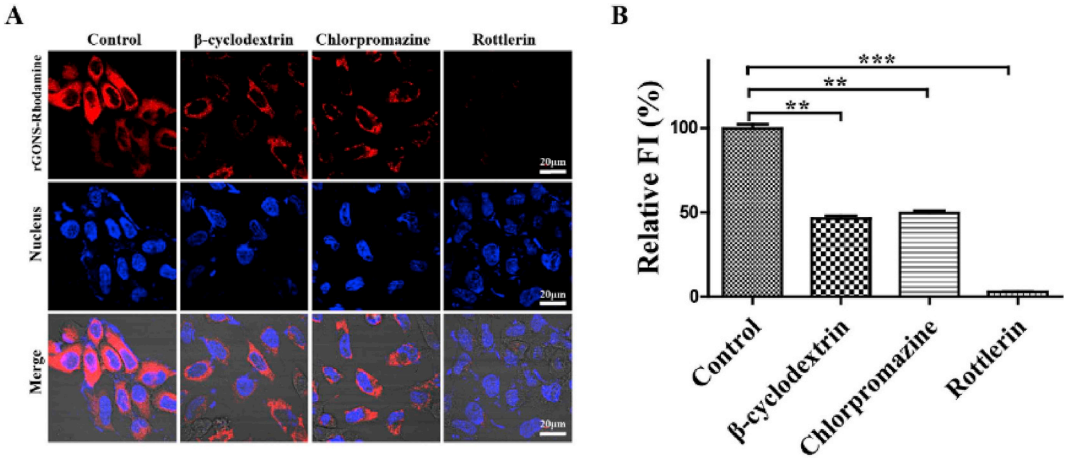

Fig. 7. Cellular trafficking and uptake mechanism of rGONS. Confocal microscopy images of the internalization and sub-cellular localization of rGONS in the presence of different inhibitors. The error bars represent the standard deviation of the three repeated experiments. *P < 0.05, **P < 0.01, ***P < 0.001.

chlorpromazine are specific inhibitors corresponding to caveolae-mediated endocytosis, clathrin-dependent endocytosis and micropinocytosis [37]. These results demonstrated that rGONS entered into cell cytosol mainly through micropinocytosis, the most economical and efficient pathway to maximize the uptake of extracellular substances [38]. According to our knowledge, this is the first report for studying the pathway of GO-based probe entering into cells, which is important for explaining the efficiency difference of cell imaging using different probe. Meanwhile, it was found that rGONS mainly located in the cytosol, the same region with mRNA, which further confirmed the

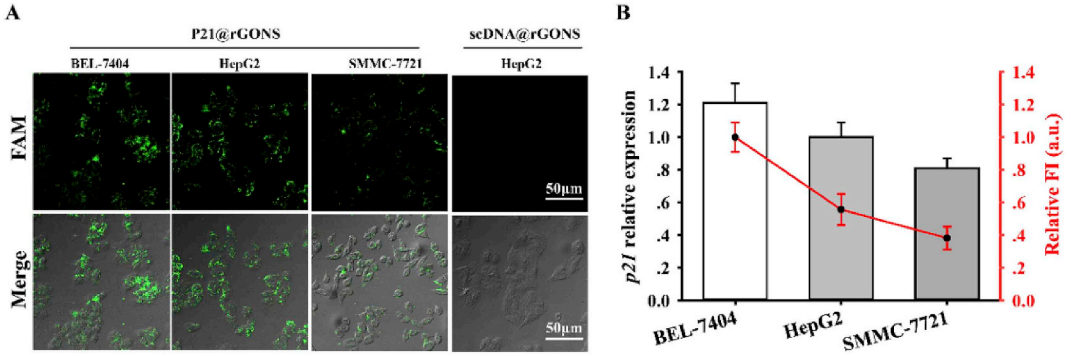

Fig. 8. Detection of p21 mRNA level in liver cancer cell lines (BEL-7404, HepG2, SMMC-7721). (A) Fluorescence images of these cell lines were taken after 8 h of incubating with P21@rGONS nanosystem or scDNA@rGONS nanosystem to cell. (B) The comparison of p21 mRNA level in different cancer cell lines obtained from P21@rGONS nanosystem and RT-PCR.

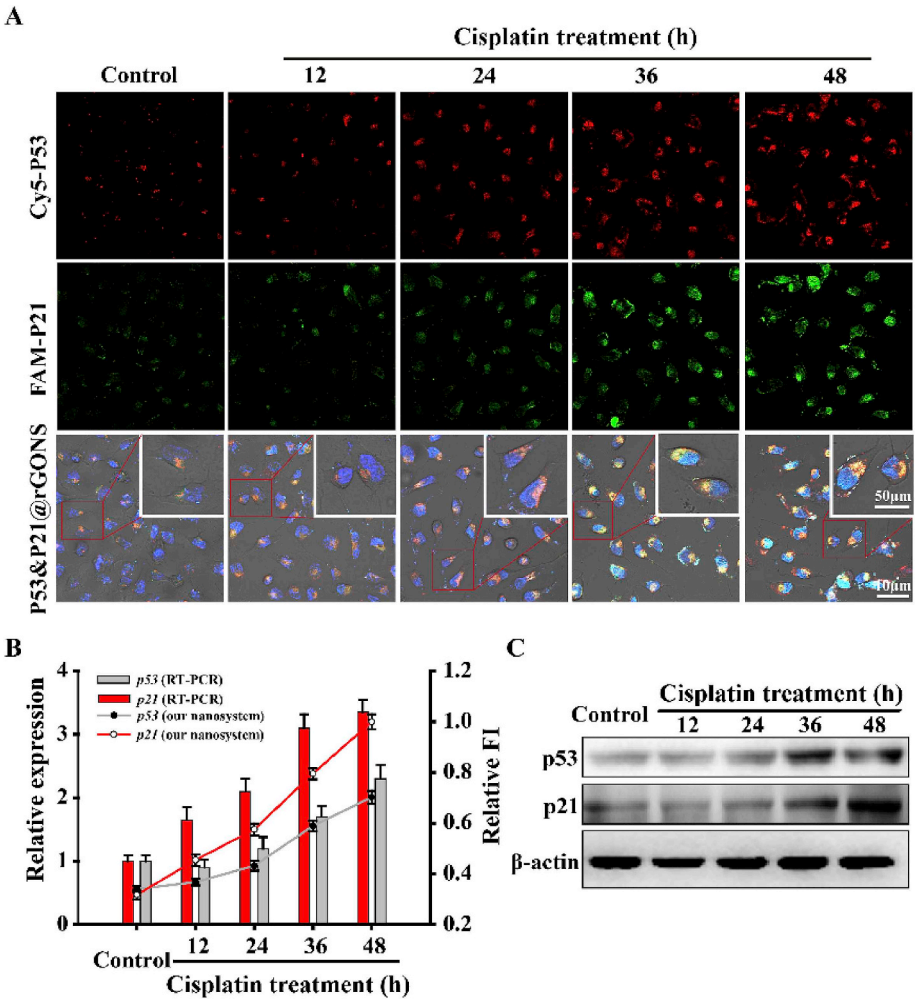

Fig. 9. p53&p21 mRNA image *in vivo* (A) As the treatment time increased from 0 to 48 h, progressively increasing fluorescence signals corresponding to P53 and P21 were visualized in HepG2 cells under laser confocal microscopy. (B) p53 and p21 mRNA assay of HepG2 cells treated with cisplatin for different time using P53& P21@rGONS detection system and RT-PCR analysis. (C) p53 and p21 protein assay of HepG2 cells treated with cisplatin for different time.

reliability of mRNA assay by using this system.

3.8. Imaging of p53&p21 mRNA in living cells

Based on the above findings, the system was used for mRNA imaging in living cells. First, we investigated the effect of incubation time on the fluorescence signal change and found that the signal positively varied with incubation time before 8 h (Fig.S6). This data clearly confirmed the high stability and the reliability of imaging in situ of the probe system by avoiding false positive signal inherited in the molecular beacon-based method [39]. Then, the p21@rGONS was used to directly characterize the difference of p21 mRNA in several kinds of tumor cell lines. Fig. 8A indicated that fluorescence intensity decreased according to the sequence of BEL-7404, HepG2 and SMMC-7721, respectively, which directly reflect the mRNA level from single cell. In the control experiment, nearly no fluorescence was observed for scDNA@

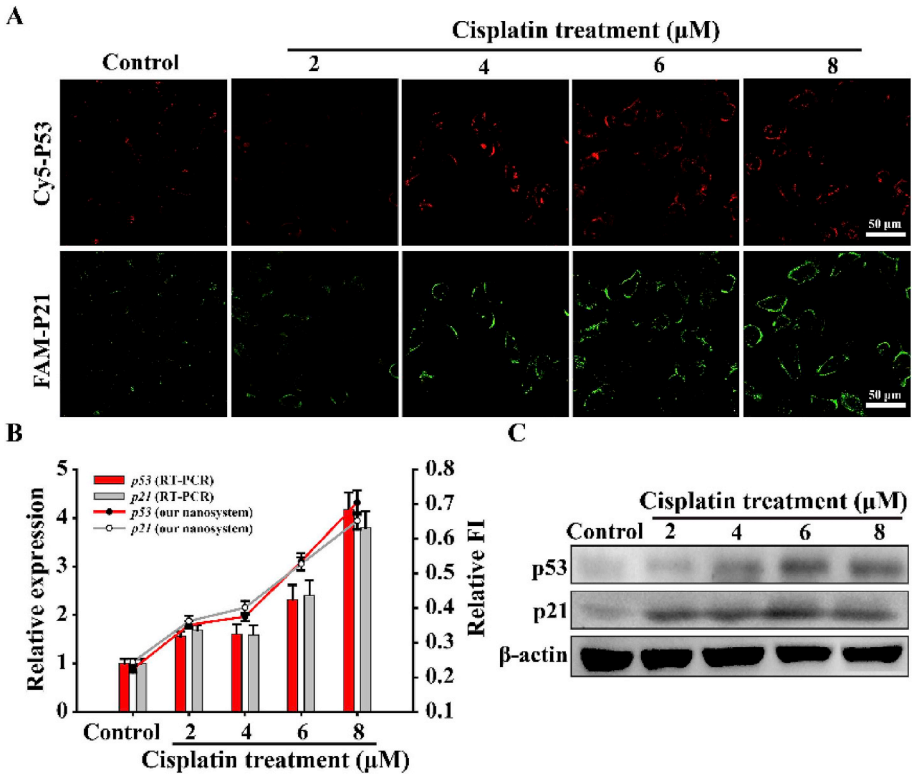

Fig. 10. Monitoring of p53&p21 mRNA in HepG2 cells treated with different concentrations of cisplatin (A) Gradually increase of fluorescence signal corresponding to p53 and p21 mRNA in HepG2 cells after with cisplatin-treatment from 0 to 8 μM. (B) p53 and p21 mRNA assay of HepG2 cells treated with cisplatin for different time using P53&P21@rGONS detection system and RT-PCR analysis. (C) Western blotting of p53 and p21protein levels in HepG2 cells treated with cisplatin for different concentrations.

rGONS nanosystem, which reflected the reliability of mRNA imaging in living cells. Meanwhile, p21 mRNA level in these cell lines (Fig. 8B, red line) were further confirmed using RT-PCR assay (Fig. 8B, bar). The consistent results between the two methods indicate that this detection system could effectively discriminate the level of p21 mRNA in different cancer cells.

3.9. Dynamic simultaneous detection of p53 and p21 mRNA

Based on the eminent performance of rGONS nanosystem for p21 mRNA image, the method was then used to simultaneous monitor the effect of cisplatin treatment on the dynamic change of p53 and p21 mRNA. As shown in Fig. 9A, both of red and green fluorescence in HepG2 cells, which correspondingly reflected the p53 and p21 mRNA levels, increased in a time- and concentration-dependent manner, which is consistent with previous report that cisplatin can upregulate level of p53 signaling pathway related mRNA [40]. Meanwhile, *in vitro* assay using P53&P21@rGONS nanosystem and RT-PCR method further confirmed the upregulation of the two genes mRNA induced by cisplatin (Fig. 9B). Moreover, cisplatin treatment can upregulate p53 and p21 protein in a concentration-dependent manner (Fig. 10). These results clearly indicate that the probe@rGONS nanosystem is hopeful for reliably monitoring the efficiency of drug treatment on the gene mRNA expression.

4. Conclusions

In this study, we developed a new nanosystem for double mRNA assay *in vitro* and *in vivo* by monitoring fluorescence signal change of nanosystem. *In vitro* assay indicated its outstanding fluorescence quenching efficiency, excellent biocompatibility, high cell uptake efficiency and strong anti-nuclease capability in living cells. Meanwhile, the nanosystem with high selectivity can rapidly detect target mRNA with a limitation of 0.71 ± 0.053 nM (p53) and 0.46 ± 0.045 nM (p21). Moreover, the nanosystem was successfully applied to monitor the regulating function of cisplatin on p53 and p21 mRNA from living cell level, which is beneficial for evaluating the efficiency of chemotherapy. In summary, this study provides a general strategy for constructing mRNAs assay system only by changing the probe sequence, which holds great potential for exploring transcription-related molecular mechanism of diseases.

Conflicts of interest

The authors declare that they have no conflict of interest, these authors contributed to the work equally and should be regarded as co-first authors.

Acknowledgement

This work was partially supported by the Natural Science Foundation of China (81374062 and 85673179), Hunan Province Universities 2011 Collaborative Innovation Center of Protection and Utilization of Hu-Xiang Chinese Medicine Resources and the National Standardization Project of Traditional Chinese Medicine (Grant ZYBZH-Y-HUN-23).

Appendix A. Supplementary data

Supplementary data to this article can be found online at https://doi.org/10.1016/j.talanta.2019.05.087.

References

[1] H. Wang, M. Naghavi, C. Allen, R.M. Barber, Z.A. Bhutta, A. Carter, D.C. Casey, F.J. Charlson, A.Z. Chen, M.M. Coates, Global, regional, and national life expectancy, all-cause mortality, and cause-specific mortality for 249 causes of death, 1980–2015: a systematic analysis for the Global Burden of Disease Study 2015 [J], The Lancet 388 (10053) (2016) 1459–1544.
[2] A. Jemal, F. Bray, M.M. Center, J. Ferlay, E. Ward, D. Forman, Global cancer statistics [J], CA A Cancer J. Clin. 61 (2) (2011) 69–90.
[3] Board, P.A.T.E., Adult Primary Liver Cancer Treatment (PDQ®), PDQ Cancer Information Summaries [Internet], National Cancer Institute (US), 2018.
[4] P. Anand, A.B. Kunnumakara, C. Sundaram, K.B. Harikumar, S.T. Tharakan, O.S. Lai, B. Sung, B.B. Aggarwal, Cancer is a preventable disease that requires major

lifestyle changes [J], Pharmaceut. Res. 25 (9) (2008) 2097–2116.
[5] M. Fischer, Census and evaluation of p53 target genes [J], Oncogene 36 (28) (2017) 3943–3956.
[6] A. Ventura, D.G. Kirsch, M.E. McLaughlin, D.A. Tuveson, J. Grimm, L. Lintault, J. Newman, E.E. Reczek, R. Weissleder, T. Jacks, Restoration of p53 function leads to tumour regression in vivo [J], Nature 445 (7128) (2007) 661–665.
[7] X.-H. Peng, Z.-H. Cao, J.-T. Xia, G.W. Carlson, M.M. Lewis, W.C. Wood, L. Yang, Real-time detection of gene expression in cancer cells using molecular beacon imaging: new strategies for cancer research [J], Cancer Res. 65 (5) (2005) 1909–1917.
[8] G.S. Pall, C. Codony-Servat, J. Byrne, L. Ritchie, A. Hamilton, Carbodiimide-mediated cross-linking of RNA to nylon membranes improves the detection of siRNA, miRNA and piRNA by northern blot [J], Nucleic Acids Res. 35 (8) (2007) e60.
[9] J.J. Chen, Key aspects of analyzing microarray gene-expression data [J], Future Medicine (2007) 473–482.
[10] E. Stylianopoulou, D. Lykidis, P. Ypsilantis, C. Simopoulos, G. Skavdis, M. Grigoriou, A rapid and highly sensitive method of non radioactive colorimetric in situ hybridization for the detection of mRNA on tissue sections [J], PLoS One 7 (3) (2012) e33898.
[11] T. Nolan, R.E. Hands, S.A. Bustin, Quantification of mRNA using real-time RT-PCR [J], Nat. Protoc. 1 (3) (2006) 1559–1582.
[12] H.D. VanGuilder, K.E. Vrana, W.M. Freeman, Twenty-five years of quantitative PCR for gene expression analysis [J], Biotechniques 44 (5) (2008) 619–626.
[13] D. Shi, F. Sheng, X. Zhang, G. Wang, Gold nanoparticle aggregation: colorimetric detection of the interactions between avidin and biotin [J], Talanta 185 (2018) 106–112.
[14] Y. Sun, Y. Wang, C. Lau, G. Chen, J. Lu, Hybridization-initiated exonuclease resistance strategy for simultaneous detection of multiple microRNAs [J], Talanta 190 (2018) 248–254.
[15] M.R. Awual, I.M. Rahman, T. Yaita, M.A. Khaleque, M. Ferdows, pH dependent Cu (II) and Pd (II) ions detection and removal from aqueous media by an efficient mesoporous adsorbent [J], Chem. Eng. J. 236 (2014) 100–109.
[16] M.R. Awual, M.M. Hasan, A. Shahat, M. Naushad, H. Shiwaku, T. Yaita, Investigation of ligand immobilized nano-composite adsorbent for efficient cerium (III) detection and recovery [J], Chem. Eng. J. 265 (2015) 210–218.
[17] M.R. Awual, Novel nanocomposite materials for efficient and selective mercury ions capturing from wastewater [J], Chem. Eng. J. 307 (2017) 456–465.
[18] M.R. Awual, A novel facial composite adsorbent for enhanced copper (II) detection and removal from wastewater [J], Chem. Eng. J. 266 (2015) 368–375.
[19] H.J. Yoon, T.H. Kim, Z. Zhang, E. Azizi, T.M. Pham, C. Paoletti, J. Lin, N. Ramnath, M.S. Wicha, D.F. Hayes, Sensitive capture of circulating tumour cells by functionalized graphene oxide nanosheets [J], Nat. Nanotechnol. 8 (10) (2013) 735–741.
[20] H. Yue, X. Zhou, M. Cheng, D. Xing, Graphene oxide-mediated Cas9/sgRNA delivery for efficient genome editing [J], Nanoscale 10 (3) (2018) 1063–1071.
[21] C. Zhao, J. Fan, L. Peng, L. Zhao, C. Tong, W. Wang, B. Liu, An end-point method based on graphene oxide for RNase H analysis and inhibitors screening [J], Biosens. Bioelectron. 90 (2017) 103–109.
[22] J. Fan, X. Zhang, Y. Cheng, C. Xiao, W. Wang, X. Liu, C. Tong, B. Liu, Increasing the sensitivity and selectivity of a GONS quenched probe for an mRNA assay assisted with duplex specific nuclease [J], RSC Adv. 7 (57) (2017) 35629–35637.
[23] L. Peng, J. Fan, C. Tong, Z. Xie, C. Zhao, X. Liu, Y. Zhu, B. Liu, An ultrasensitive fluorescence method suitable for quantitative analysis of mung bean nuclease and inhibitor screening in vitro and vivo [J], Biosens. Bioelectron. 83 (2016) 169–176.
[24] K. Erickson, R. Erni, Z. Lee, N. Alem, W. Gannett, A. Zettl, Determination of the local chemical structure of graphene oxide and reduced graphene oxide [J], Adv. Mater. 22 (40) (2010) 4467–4472.
[25] G. Xi, X. Wang, T. Chen, A reduced graphene oxide-based fluorescence resonance energy transfer sensor for highly sensitive detection of matrix metalloproteinase 2 [J], Int. J. Nanomed. 11 (2016) 1537–1547.
[26] R. Li, L.M. Guiney, C.H. Chang, N.D. Mansukhani, Z. Ji, X. Wang, Y.-P. Liao, W. Jiang, B. Sun, M.C. Hersam, Surface oxidation of graphene oxide determines membrane damage, lipid peroxidation, and cytotoxicity in macrophages in a pulmonary toxicity model [J], ACS Nano 12 (2) (2018) 1390–1402.
[27] C. Lu, P.J. Huang, B. Liu, Y. Ying, J. Liu, Comparison of graphene oxide and reduced graphene oxide for DNA adsorption and sensing [J], Langmuir 32 (41) (2016) 10776–10783.
[28] M.G. Kim, J.Y. Park, W. Miao, J. Lee, Y.K. Oh, Polyaptamer DNA nanothread-anchored, reduced graphene oxide nanosheets for targeted delivery [J], Biomaterials 48 (2015) 129–136.
[29] Y.-H. Wang, H.-H. Deng, Y.-H. Liu, X.-Q. Shi, A.-L. Liu, H.-P. Peng, G.-L. Hong, W. Chen, Partially reduced graphene oxide as highly efficient DNA nanoprobe [J], Biosens. Bioelectron. 80 (2016) 140–145.
[30] C. Zhao, Y. Chen, J. Fang, J. Fan, C. Tong, X. Liu, B. Liu, W. Wang, DNase-targeted natural product screening based on a sensitive and selective DNase I detecting system [J], RSC Adv. 7 (49) (2017) 30911–30918.
[31] H. Liu, J. Fan, W. Liu, C. Tong, Z. Xie, R. Deng, X. Long, A dual signal amplification method for miR-204 assay by combining chimeric molecular beacon with double-stranded nuclease [J], Analytical Methods 10 (48) (2018) 5834–5841.
[32] S.-R. Ryoo, J. Lee, J. Yeo, H.-K. Na, Y.-K. Kim, H. Jang, J.H. Lee, S.W. Han, Y. Lee, V.N. Kim, Quantitative and multiplexed microRNA sensing in living cells based on peptide nucleic acid and nano graphene oxide (PANGO) [J], ACS Nano 7 (7) (2013) 5882–5891.
[33] C. Lu, Hua hyphen, H. Yang, Hao hyphen, C. Zhu, Ling hyphen, X. Chen, G. Chen, Nan hyphen, A graphene platform for sensing biomolecules [J], Angew. Chem. 121 (26) (2009) 4879–4881.
[34] C.H. Lu, C.L. Zhu, J. Li, J.J. Liu, X. Chen, H.H. Yang, Using graphene to protect DNA from cleavage during cellular delivery [J], Chem. Commun. 46 (18) (2010) 3116–3118.
[35] W. Pan, B. Liu, X. Gao, Z. Yu, X. Liu, N. Li, B. Tang, A graphene-based fluorescent nanoprobe for simultaneous monitoring of miRNA and mRNA in living cells [J], Nanoscale 10 (29) (2018) 14264–14271.
[36] J. Li, X. Zhang, J. Jiang, Y. Wang, H. Jiang, J. Zhang, X. Nie, B. Liu, Systematic assessment of the toxicity and potential mechanism of graphene derivatives in vitro and in vivo [J], Toxicol. Sci. 167 (1) (2018) 269–281.
[37] J. Conde, N. Oliva, M. Atilano, H.S. Song, N. Artzi, Self-assembled RNA-triple-helix hydrogel scaffold for microRNA modulation in the tumour microenvironment [J], Nat. Mater. 15 (3) (2016) 353–363.
[38] F. Zhao, Y. Zhao, Y. Liu, X. Chang, C. Chen, Y. Zhao, Cellular uptake, intracellular trafficking, and cytotoxicity of nanomaterials [J], Small 7 (10) (2011) 1322–1337.
[39] A.K. Chen, M.A. Behlke, A. Tsourkas, Avoiding false-positive signals with nuclease-vulnerable molecular beacons in single living cells [J], Nucleic Acids Res. 35 (16) (2007) e105.
[40] K. Qu, T. Lin, J. Wei, F. Meng, Z. Wang, Z. Huang, Y. Wan, S. Song, S. Liu, H. Chang, Cisplatin induces cell cycle arrest and senescence via upregulating P53 and P21 expression in HepG2 cells [J], Nan Fang Yi Ke Da Xue Xue Bao 33 (9) (2013) 1253–1259.